Int. J. Electrochem. Sci., 6 **(2011)** 5287 - 5297

International Journal of
ELECTROCHEMICAL
SCIENCE
www.electrochemsci.org

Microstructure Changes of Amorphous Mg-Ni-Nd Alloys During Charge/Discharge Cycling and its Thermodynamic Verification

Huang Lin-jun[*], *Wang Yan-xin, Tang Jian-guo, Liu Jing-quan, Wang Yao, Liu Ji-xian*

(College of Chemistry, Chemical and Environmental Engineering, Laboratory of New Fiber Materials and Modern Textile, the Growing Base for State Key Laboratory, Qingdao University, Qingdao 266071, China)
[*]E-mail: newboy66@126.com

Received: 29 August 2011 / *Accepted:* 17 October 2011 / *Published:* 1 Novembar 2011

Amorphous Mg-based hydrogen-storage alloy $(Mg_{70.6}Ni_{29.4})_{90}Nd_{10}$ is prepared by melt-spinning. The phase structures of the ribbons before and after charge/discharge cycling are characterized by high-resolution transmission electron microscopy (HRTEM), X-ray diffraction (XRD) analysis, respectively. It is found that the amorphous structure begins to crystallize after four cycles of hydrogenation/ dehydrogenation and a new nano-crystallized phase $NdMg_2Ni_9$ is detected with average grain size in the range 5 nm. Nano-size Mg_2Ni phases appear after 6–10 cycles，and after 20 cycles of charging/discharging stable Mg_2Ni, α-Mg and Nd_2H_5 phases are present. The following results of thermodynamics calculation verifies that the nano-crystallized phase $NdMg_2Ni_9$ is present firstly during the process of crystallization, because it's free-energy (ΔG=-15.2789KJ/mol，T=300K) is the lowest among Mg-Ni phase（ΔG=-8.2694KJ/mol， T=300K）and Mg-Nd phase（ΔG=-13.29503KJ/mol，T=300K）. A good cycle life and high discharge capacity are also observed in the $(Mg_{70.6}Ni_{29.4})_{90}Nd_{10}$ alloy electrode. It is suggested that homogeneous microstructure contributes to the enhancement in electrochemical characteristics; the presence of $NdMg_2Ni_9$ is beneficial for the improvement in cycle life of $(Mg_{70.6}Ni_{29.4})_{90}Nd_{10}$ alloy electrode.

Keywords: Mg-Ni-Nd hydrogen-storage alloy; microstructure; thermodynamics; discharge capacity.

1. INTRODUCTION

Mg-based hydrogen storage alloys are considered as one of the most promising candidates of third generation alloys, because of their high discharge capacity, lower density and rich natural resources [1–3]. The microstructure and hydrogen storage properties of Mg_2Ni hydrides such as

Mg_2NiH_4 [4, 5] were extensively investigated. However, their poor dehydrogenation kinetics at room temperature and serious degradation of the discharge capacity during electrochemical cycles cause them to be far from practical applications. In recent years, special attention has been given to the microstructure of the electrode and the amorphous structure was known as a key factor to achieve high discharge capacity and good cycling stability for its special disordered atomic packing and good corrosion resistance [6–8].

However, the amorphous structure is unstable and would be crystallized with the proceeding of charge/discharge cycles. In addition, details of the microstructure evolution of Mg-based amorphous alloys processed by hydrogenation/dehydrogenation are not clear. Therefore, how to retain the amorphous structure of the electrode or postpone the crystallization of the amorphous electrode materials becomes very important in future studies.

In a series of our previous papers the crystallization, microstructure and the hydrogen storage properties for various rapidly Mg-based amorphous alloys were studied [9–11]. This paper is a further study aiming to give a detailed investigation on the microstructure evolution and its thermodynamics calculation of amorphous $(Mg_{70.6}Ni_{29.4})_{90}Nd_{10}$ alloy processed by hydrogenation/dehydrogenation, and the effects of microstructure on the discharge capacity are also discussed.

2. EXPERIMENTAL

$(Mg_{70.6}Ni_{29.4})_{90}Nd_{10}$ alloy ingot was prepared by induction melting a mixture of pure Nd metal and Mg-Ni alloy in a vacuum furnace under the protection of argon gas. Based on the low melting point and the high vapor pressure of Mg, a special melting technique, that is positive pressure protection and repeated melting, has to be taken to prevent massive Mg evaporation and ensure composition homogeneity during master alloy ingot preparation. The amorphous ribbons were produced by a single roller melt-spun technique (copper quenching disc with a diameter of 250mm and surface velocity of about $39ms^{-1}$) in a argon atmosphere of 400mbar. The ribbons were about 2mm wide and 20 μm thick.

In electrochemical measurement, the amorphous alloy ribbons were fixed in a special mold to form the negative electrode. The positive electrode was made of Ni-oxyhydroxide/dihydroxide. The alkaline solution was 6mol/l KOH containing 20g/l LiOH. The specimens were charged at $100mAg^{-1}$ for 12h and discharged at $50mAg^{-1}$ using the BTW-2000 battery testing instrument (Arbin). The discharged cut-off potential was set to 0.8 V between the two electrodes. The resting time between the charge and discharge was 1 h.

The microstructural characterization of the ribbons after charge/discharge cycles was confirmed by high resolution transmission electron microscopy (HRTEM, JEOL-2010) and by X-ray (using Cu k_α radiation) and electron diffraction.

3. RESULTS AND DISCUSSION

3.1 Microstructure evolution

The XRD patterns of the amorphous samples that charging/discharging for one to six cycles are presented in Fig.1. It is seen that after one to three cycles of charging/discharging (Fig.1 (a), (b) and (c)) the samples show only a broad and diffuse peak, namely the featureless appearance is typical of amorphous structure.

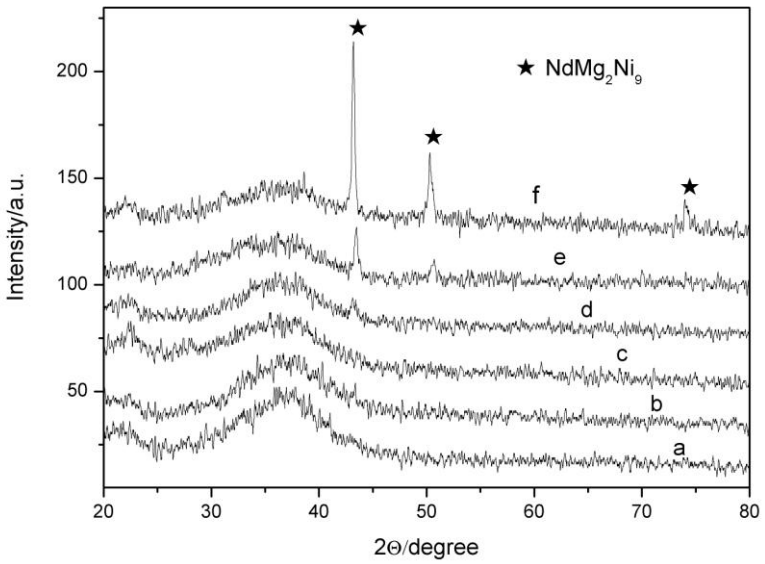

Figure 1. XRD patterns of amorphous $(Mg_{70.6}Ni_{29.4})_{90}Nd_{10}$ samples charge/discharge for: (a) one cycle; (b) two cycles; (c) three cycles; (d) four cycles; (e) five cycles; (f) six cycles.

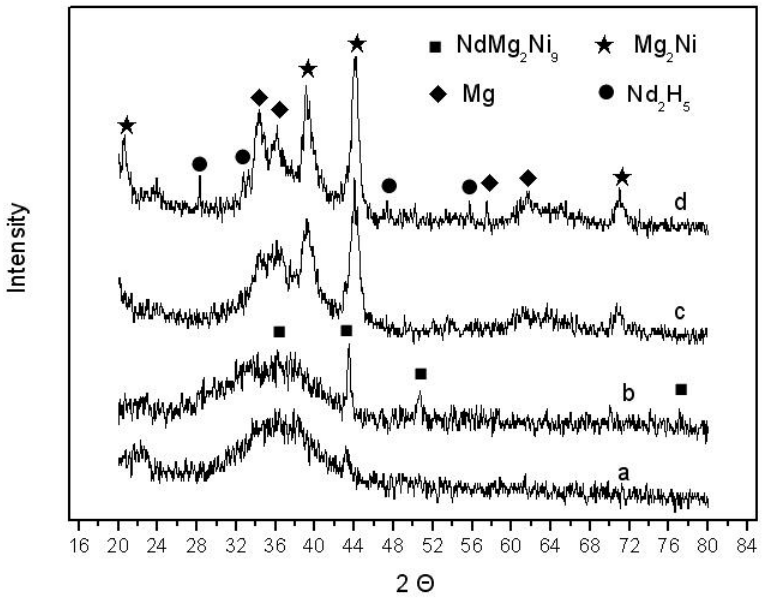

Figure 2. XRD patterns of amorphous samples $(Mg_{70.6}Ni_{29.4})_{90}Nd_{10}$ charge/discharge for: (a) five cycles; (b) six cycles; (c) ten cycles; (d) twenty cycles.

However, after four cycles of hydrogenation/dehydrogenation, the amorphous structure begins to nano-crystallize (see Fig.1 (d)). By indexing, the nano-crystalline phase $NdMg_2Ni_9$ is detected. The peak of the new phase showed in Fig.1 (e) and (f) becomes strong more and more with the proceeding of charge/discharge cycles, indicating that the new phase $NdMg_2Ni_9$ is growing.

The XRD patterns of the amorphous samples that charging/discharging for five, six, ten and twenty cycles are presented in Fig.2. It is seen that the amorphous structure is crystallized gradually with the proceeding of the charge/discharge cycles. Nano-size phases Mg_2Ni appear in the six to ten cycles. After twenty cycles of charging/discharging the stable Mg_2Ni, α-Mg and Nd_2H_5 phases are present (Fig.2 (d)), indicating that the phase $NdMg_2Ni_9$ formed at beginning is decomposed into phases Mg_2Ni, α-Mg and Nd_2H_5 gradually with the proceeding of hydrogenation/dehydrogenation.

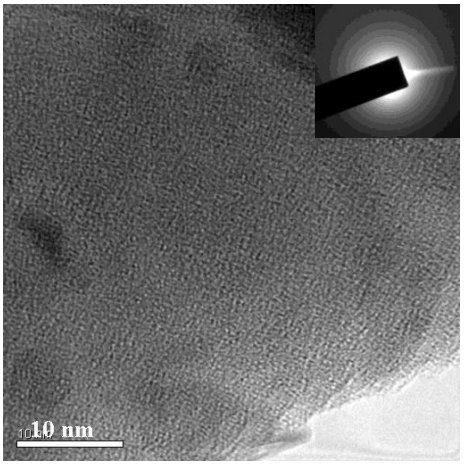

Figure 3. HRTEM image and electron diffraction pattern of amorphous sample $(Mg_{70.6}Ni_{29.4})_{90}Nd_{10}$ charged/discharged for three cycles.

The HRTEM image and electron diffraction pattern of amorphous sample $(Mg_{70.6}Ni_{29.4})_{90}Nd_{10}$ charged/discharged for three cycles are showed in Fig.3. It is found that a uniform amorphous structure was obtained after three cycles of hydrogenation/dehydrogenation. (The size of short-range order structure in the amorphous is about 0.5nm)

Fig. 4 showed the HRTEM image and electron diffraction pattern of amorphous sample $(Mg_{70.6}Ni_{29.4})_{90}Nd_{10}$ charged/discharged for six cycles. It is seen that charging/discharging after six cycles for the amorphous samples leads to formation of nano-crystalline phase $NdMg_2Ni_9$ with average grain size in the range 10-20 nm (Fig. 2 (b) and Fig. 4(c)) and the nano-size phase Mg_2Ni appears with average grain size in the range 5-15 nm (Fig. 4 (a) and (b)).

Fig. 5 showed the HRTEM image and electron diffraction pattern of amorphous sample $(Mg_{70.6}Ni_{29.4})_{90}Nd_{10}$ charged/discharged for ten cycles. It exhibits that amorphous sample that charged/discharged hydrogen after 10 cycles results in the formation of nanocrystals structures besides a few residual amorphous phases. Charging/discharging after ten cycles causes formation of a coarser grained crystalline phase Mg_2Ni with average grain size in the range 15-30 nm (Fig.2 (c) and Fig. 5).

The HRTEM image and electron diffraction pattern of amorphous sample $(Mg_{70.6}Ni_{29.4})_{90}Nd_{10}$ charged/discharged for twenty cycles are showed in Fig.6.

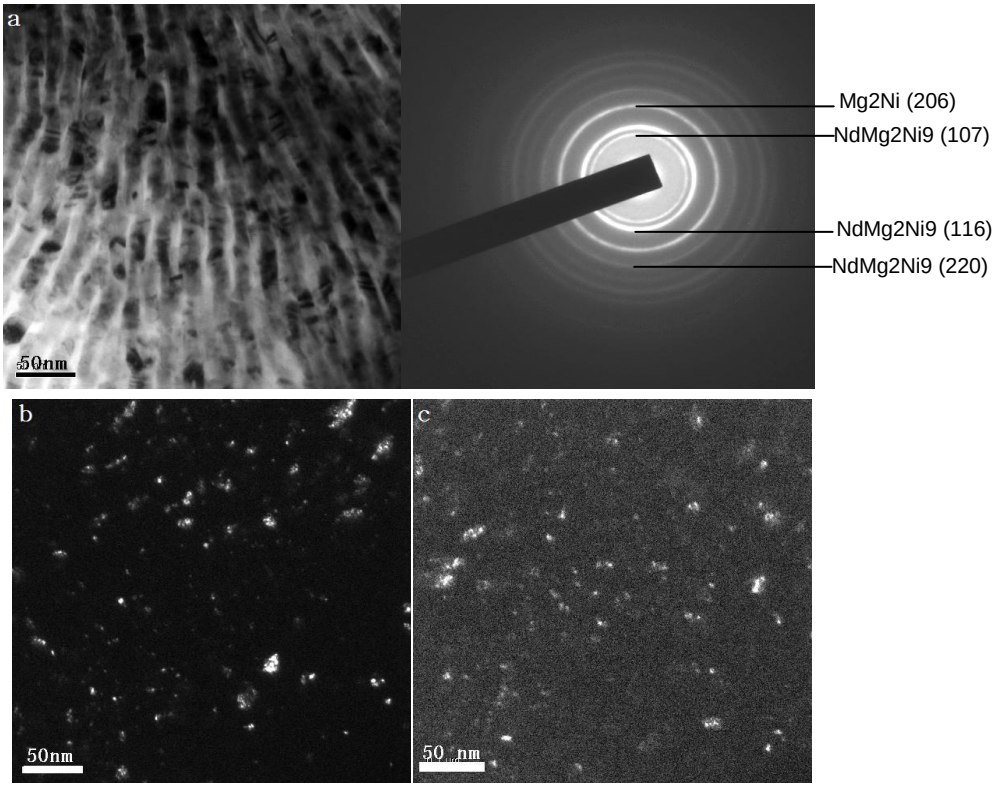

Figure 4. HRTEM analysis of amorphous sample $(Mg_{70.6}Ni_{29.4})_{90}Nd_{10}$ charged/discharged for six cycles: (a) bright filed image and electron diffraction; (b) dark filed image of Mg_2Ni; (c) dark filed image of $NdMg_2Ni_9$.

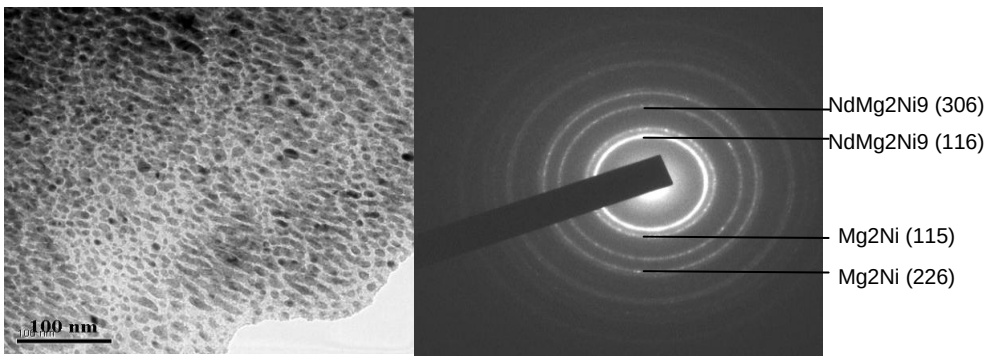

Figure 5. HRTEM image and electron diffraction pattern of amorphous sample $(Mg_{70.6}Ni_{29.4})_{90}Nd_{10}$ charged/discharged for ten cycles.

It is found that after twenty cycles of charging/discharging the amorphous samples are almost completely crystallized and stable Mg_2Ni, α-Mg and Nd_2 H_5 phases with the biggest grain size about 100 nm (Fig. 6) are present, indicating that the $NdMg_2Ni_9$ phase formed at beginning is decomposed into Mg_2Ni, α-Mg and Nd_2H_5 phases gradually with the proceeding of hydrogenation/dehydrogenation (Fig.2 and Fig.6).

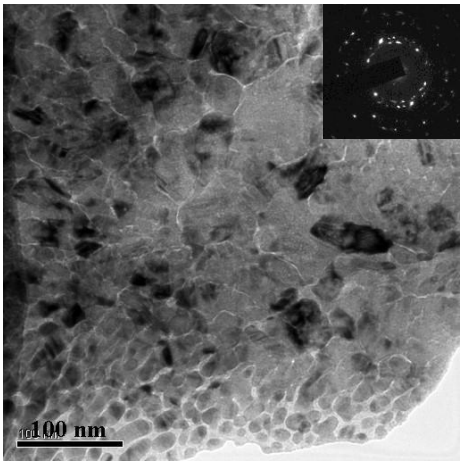

Figure 6. HRTEM image and electron diffraction pattern of amorphous sample $(Mg_{70.6}Ni_{29.4})_{90}Nd_{10}$ charged/discharged for twenty cycles.

3.2 Thermodynamics calculation

As we known, crystallization procedure of amorphous alloy in the nucleation process is affected by the Energy and Structural fluctuations, and the formation of various phases abides by the lowest energy principle. According to our previous results[12], The feasible composition are (1) 80at.%Mg_2Ni+20 at.% MgNd, (2)35at.% $NdMg_2Ni_9$+65at.% $Mg_{41}Nd_5$ after $(Mg_{70.6}Ni_{29.4})_{90}Nd_{10}$ hydrogen storage amorphous alloy crystallization.

According to Miedema [13, 14] semi-empirical theory and the extended model proposed by Zhang Bangwei [15], we calculated the Gibbs free energy ΔG (see Table 1) of $NdMg_2Ni_9$, Mg-Ni, Mg-Nd alloys, and the forming hydride MgH_2, Nd_2H_5 in the discharge process. The Required calculating parameters are shown in Table 2.

For the alloy combined by A and B constituents, the energy of mixing is given by

$$\Delta H^0_{iinj} = 2PV_i^{2/3} \Big/ (n_i^{-1/3} + n_j^{-1/3}) \times \left[-(\Delta\Phi^*)^2 + Q \Big/ P(\Delta n^{1/3})^2 - R/P \right] \qquad (1)$$

where V, Φ* and n are the parameters, P, Q and R are the constants determined by Miedema. For a ternary alloy, only the binary interaction between atoms is considered, and the ternary atomic interactions between the constituents are neglected when the Miedema model extends to the ternary alloys. Then, the chemical interaction contribution is given by

$$\Delta H_{ABC}^{M} = \Delta H_{AB} + \Delta H_{BC} + \Delta H_{AC} \quad (2)$$

$$\Delta H_{ij} = x_i x_j (x_j \Delta H^{0}_{iinj} + x_i \Delta H^{0}_{jini}) \quad (3)$$

where x_i and x_j are the atomic compositions species i and j respectively.

Similarly, only the binary contribution is considered in the elastic term, so the elastic contribution in a ternary alloy is given by

$$\Delta \mathrm{H}^{\mathrm{e}}_{\mathrm{ABC}} = \Delta H^{e}_{AB} + \Delta H^{e}_{BC} + \Delta H^{e}_{AC} \quad (4)$$

$$\Delta \mathrm{H}^{\mathrm{e}}_{\mathrm{ij}} = x_i x_j (x_j \Delta H^{e}_{iinj} + x_i \Delta H^{e}_{jini}) \quad (5)$$

where $\Delta \mathrm{H}^{\mathrm{e}}_{\mathrm{ij}}$ is the size-mismatch contribution to the formation enthalpy in a binary system. The Friedel formula [16] is used in the present study, given by

$$\Delta \mathrm{H}^{\mathrm{e}}_{\mathrm{iinj}} = 24\pi B_i u_j R_i R_j (R_i - R_j)^2 / (3B_i R_j + 4u_j R_i) \quad (6)$$

where B_i is the bulk modulus of the solute, and u_j is the shear modulus of the solvent. The values of B and u for elements have been tabulated by Gschneidner [17]. R_i and R_j are the radii for solute and solvent atoms, respectively.

The formation energy of a ternary alloy system can then be given by

$$\Delta \mathrm{H}^{\mathrm{MF}}_{\mathrm{ABC}} = \Delta H^{M}_{ABC} + \Delta H^{e}_{ABC} \quad (7)$$

The results of Table 2 show that, the free energy of $NdMg_2Ni_9$ (ΔG =- 15.2789 KJ/mol, T = 300K) is lower than that of Mg-Ni and Mg-Nd alloy.

Table 1. The computation parameter of ΔG for each compound

element	Φ*/V	$n^{1/3}_{1/3}$/(d.u.)	V/(cm^3/mol)	R/P/(V^2)	Tm/K	$V^{2/3}$/(cm^2/mol)
Mg	3.45	1.17	13.97	0.4	922	5.81
Ni	5.2	1.75	6.593	1	1726	3.52
Nd	3.19	1.2	20.59	0.7	1289	7.51

Therefore, the phase of $NdMg_2Ni_9$ firstly occurring during the crystallization process is entirely possible. If $NdMg_2Ni_9$ alloy can be stable in the matrix, the 1mol $(Mg_{70.6}Ni_{29.4})_{90}Nd_{10}$ could be composed of 35at.% $NdMg_2Ni_9$ +65 at.% $Mg_{41}Nd_5$, their system ΔG =- 8.3998 KJ /mol. However, for

system 80at.% Mg_2Ni +20 at.% MgNd, their system ΔG =- 9.4056KJ/mol, which is more stable than above-mentioned.

Table 2. Δ G of $NdMg_2Ni_9$、Mg-Ni、Mg-Nd、MgH_2 and Nd-H compounds(T=300k)

Compounds	Δ G/(KJ/mol)	Compounds	Δ G/(KJ/mol)
$NdMg_2Ni_9$	-15.2789	MgH_2	-97.6573
Mg_2Ni	-8.2694	Nd_2H_5	-133.1630
$Mg_{41}Nd_5$	-4.6956	MgNd	-13.9503

Therefore, in the long-term charge-discharge cycling conditions, $NdMg_2Ni_9$ phase crystallized in the primary would be decomposed into Mg_2Ni and MgNd phase. When hydrogen atoms enter MgNd phase in hydrogenation, MgNd phase would be decomposed into MgH_2 and Nd_2H_5. The Nd_2H_5 phase is stable (ΔG =- 133.1630KJ/mol) [18], so the the final detected phase are Mg_2Ni, α-Mg and Nd_2H_5.

3.3 Effects of microstructure on discharge capacity

Fig. 7 shows the variation of the discharge capacity of the $(Mg_{70.6}Ni_{29.4})_{90}Nd_{10}$ sample versus the number of cycles. It can be observed that with increasing cycle number the capacity reached a maximum after three cycles, and then decreased in higher cycles. It suggests that the first two cycles are activation process. This phenomenon has been observed in other Mg-based hydrogen storage alloys [19, 20]. The largest discharge capacity of the sample reached 580.5mAhg^{-1} after three cycles, and then decreased for next cycles. After 10 cycles, capacity falloff was regular. The capacity after 20 cycles (460.9mAhg^{-1}) reaches 80% of the maximum capacity.

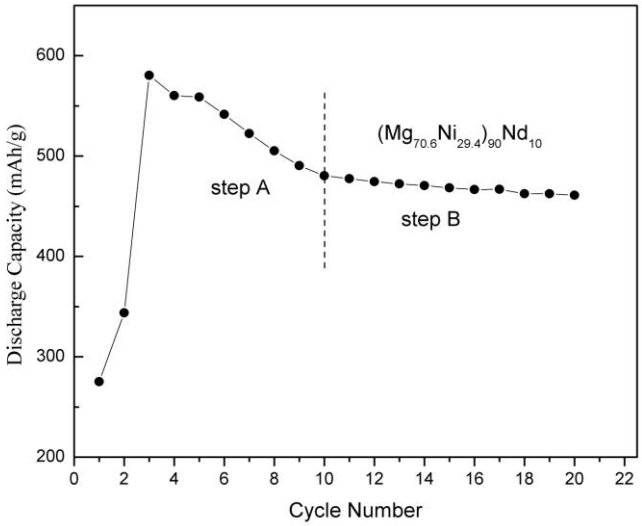

Figure 7. Variation of the discharge capacity versus the cycle number for the $(Mg_{70.6}Ni_{29.4})_{90}Nd_{10}$ samples

As shown in Fig. 7, the drop-off of discharge capacity could be divided into two steps according to the decay rate of discharge capacity, i.e. from the 3rd to the 10th cycles as the step A and from the 10th to the 20th cycles as the step B. The first step corresponds to the formation and the decomposition of $NdMg_2Ni_9$ as well as the formation of Mg_2Ni, while the second step corresponds to the presence of Mg_2Ni, α-Mg and Nd_2H_5 (Figs.2 and 6). This indicates that $NdMg_2Ni_9$ contributes to a higher discharge capacity than Mg_2Ni, α-Mg and Nd_2H_5. Therefore, a conclusion could be drawn that the crystallization of amorphous $(Mg_{70.6}Ni_{29.4})_{90}Nd_{10}$ alloy is also responsible for the degradation of the discharge capacity.

Xuezhang et al. [21] and B.Khorkounov et al. [22] reported that the amorphous 2Mg-Fe+150wt.%Ni (the maximum discharge capacity is 565.2mAhg^{-1})and $Mg_{61}Ni_{30}Y_9$ ribbons (the maximum discharge capacity is 570mAhg^{-1}) were synthesized by mechanical alloying. Wang et al. [23], Xu et al. [24] and Jurczyk et al. [25] also reported respectively that the amorphous $Mg_{1.8}Nd_{0.2}Ni$ (the discharge capacity is 323.5mAhg^{-1}), $PrMgNi_4$ (the discharge capacity is 254mAhg^{-1}) and $Mg_{1.5}Mn_{0.5}Ni$ ribbons (the discharge capacity is 241mAhg^{-1}) were synthesized by mechanical alloying. From the above results, it is evident that the melt-spun ribbon $(Mg_{70.6}Ni_{29.4})_{90}Nd_{10}$ showed superior hydrogenation kinetics and higher discharge capacity. One explanation for this could be the homogeneous microstructure of the melt-spun alloy. The as-cast eutectic alloy charged/discharged for some cycles consisted of lamellae of primary and secondary phases (see Figs. 2 and 4), where long continuous boundaries between primary and secondary phases could act as diffusion paths prior to hydrogen diffusion into the bulk. Zhu et al. [26] also reported that an auto-catalytic effect is might govern the hydriding mechanism of the nanophase composite, while the hydriding process of single component alloys proceeds by means of a nucleation and growth mechanism. Another explanation could be the existence of nano-crystalline phase $NdMg_2Ni_9$ (see Figs. 2, 4 and 5). The new ternary Mg-based hydrogen storage alloys, RMg_2Ni_9 (where R = La, Ce, Pr, Nd, Sm and Gd), were first reported by Kadir et al. [27] in 1997, and the latest investigations of the RMg_2Ni_9 hydrogen storage alloys suggested that the new ternary alloys may be regarded as the most promising candidate for possible improvement because of their special structure for hydrogen storage [28–31]. From the above results, after four cycles of hydrogenation/dehydrogenation, the amorphous structure begins to nano-crystallize (see Figs. 1(d) and 4) and a nano-crystallized phase $NdMg_2Ni_9$ is present, rapidly leading to a very high discharge capacity (see Fig. 7). In addition, the amorphous phase embedding the nanocrystalling grains in the melt-spun material (see Figs. 4 and 5) may provide fast bulk diffusion of hydrogen because of the lower atomic density in the amorphous state. According to the results of Orimo et al. [32] reported, hydrogen concentrations in the grain boundaries are much higher than that in the grain interior and amorphous regions. The formation of nanocrystalline grains increases the grain boundary in the melt-spun ribbon sample, which no doubt promotes its hydrogen storage properties.

4. CONCLUSIONS

A detailed investigation on the microstructure evolution and its thermodynamics calculation of amorphous $(Mg_{70.6}Ni_{29.4})_{90}Nd_{10}$ alloy processed by hydrogenation/dehydrogenation was given, and the

effects of microstructure on the discharge capacity are also discussed. The results obtained are summarized as follows:

1. After four cycles of hydrogenation/dehydrogenation, the amorphous structure begins to crystallize and a nano-crystalline phase $NdMg_2Ni_9$ is detected with average grain size in the range 5-10 nm. Nano-size phases Mg_2Ni appear in the six to ten cycles.

2. After twenty cycles of charging/discharging the stable Mg_2Ni, α-Mg and Nd_2H_5 phases are present, indicating that the $NdMg_2Ni_9$ phase formed at beginning is decomposed into Mg_2Ni, α-Mg and Nd_2H_5 phases gradually with the proceeding of hydrogenation/dehydrogenation.

3. The results of thermodynamics calculation verified that the nano-crystallized phase $NdMg_2Ni_9$ was present firstly during the process of crystallization, because it's free-energy (ΔG=-15.2789KJ/mol，T=300K) is the lowest among Mg-Ni phase（ΔG=-8.2694KJ/mol，T=300K）and Mg-Nd phase（ΔG=-13.29503KJ/mol，T=300K）.

4. The discharge capacity becomes low gradually with the crystallization proceeding of amorphous structure. It indicated that the amorphous structure was a key factor to achieve high discharge capacity and good cycling stability.

ACKNOWLEDGEMENTS

This work was supported by the China Postdoctoral Science Foundation (Grant No. 20100481299), Ph.D. Fund of Shandong Province(Grant No. BS2009Cl039), Shandong Postdoctoral Innovation Fund (Grant No. 201003050) and Colleges and universities in Shandong Province science and technology projects Fund(Grant No. J11LD03).

References

1. J.C. Bolcich, A.A. Yawuy, H.L. Corso, H.A. Pertti, C.O. Anala, *Int. J. Hydrogen Energy* 19 (1994) 605.
2. L. Schlapbach, A. ZÜttel, *Nature* 414 (2001) 353.
3. N. Cui, B. Luan, H.J. Zhao, H.K. Liu, S.X. Dou, *J. Power Source* 55 (1995) 263.
4. G.N. Garcia, J.P. Abriata, J.O. Sofo, *Phys. Rev*. B 65 (2002) 064306.
5. J. Zhang, D.W. Zhou, L.P. He, P. Peng, J.S. Liu, *J. Phys. Chem. Solids* 70 (2009) 32.
6. J.-W. Liu, L.-F. Jiao, H.-T. Yuan, Y.-J. Wang, Q. Liu, *J. Alloys Comp*. 403 (2005) 270.
7. B. Khorkounov, A. Gebert, Ch. Mickel, L. Schultz, *J. Alloys Comp*. 416 (2006) 110.
8. X. Xiao, X.Wang, L. Gao, L.Wang, C. Chen, *J. Alloys Comp*. 413 (2006) 312.
9. L.J. Huang, G.Y. Liang, Z.B. Sun, *J. Alloys Comp*. 421 (2006) 279.
10. L.J. Huang, G.Y. Liang, Z.B. Sun, Y.F. Zhou, D.C.Wu, *Mater. Sci. Eng*. B 141 (2007) 121.
11. L.J. Huang, G.Y. Liang, Z. B.Sun, Y.F. Zhou，*J. Alloys Comp*. 432 (2007) 172.
12. D.C. Wu, L.J. Huang, G.Y. Liang**,** *Acta Physica Sinica*, 57 (2008)1813.
13. A.R. Miedema, *J. Less-Common Met*. 32 (1973) 117.
14. A.R. Miedema, P.F. de Chatel, F.R. de Boer, *Physica* B.100 (1980) 1.
15. Zhang Bangwei, W.A.Jesser, *Physica B*. 315 (2002) 123
16. J. Friedel, *Adv. Phys*. 3 (1954) 446.
17. K.A. Gschneidner Jr, *Solid State Phys*. 16 (1964) 275.
18. Jingtian Yin, Kazuhide Tanaka, Nobuo Tanaka, *Materials Transaction*, 43(2002)41.
19. S. Orimo, H. Fujii, K. Ikeda, *Acta Mater*. 45 (1997) 331.
20. W.H. Liu, H.Q.Wu, Y.Q. Lei, *J. Alloys Comp*. 252 (1997) 234.

21. Xuezhang xiao, Xinhua Wang, Linhui Gao, Li Wang, Changpin Chen, *J. Alloys Compd*. 413 (2006) 312.
22. B. Khorkounov, A. Gebert, Ch. Mickel, L. Schultz, *J. Alloys Compd*. 458 (2008) 479.
23. Z.M. Wang, H.Y. Zhou, Z.F. Gu, G. Cheng, A.B. Yu, *J. Alloys Compd*. 381 (2004)234–239.
24. X. Xu, H.Y. Zhou, R.P. Zou, S.L. Zhang, Z.M. Wang, *J. Alloys Compd*. 396 (2005)247–250.
25. M. Jurczyk, L. Smardz, I. Okonska, E. Jankowska, M. Nowak, K. Smardz, *Int. J. Hydrogen Energy* 33 (2008) 374–380.
26. M. Zhu, Y. Gao, Z.X. Che, Y.Q. Yang, C.Y. Chuang, *J. Alloys Compd*. 330–332 (2002)708.
27. K. Kadir, T. Sakai, I. Uehara, *J. Alloys Compd*. 257 (1997) 115.
28. K. Kadir, T. Sakai, I. Uehara, *J. Alloys Compd*. 302 (2000) 112.
29. Z.M. Wang, H.Y. Zhou, G. Cheng, Z.F. Gu, *J. Alloys Compd*. 384 (2004)279.
30. X. Xu, H.Y. Zhou, R.P. Zou, S.L. Zhang, Z.M. Wang, *J. Alloys Compd*. 396 (2005)247.
31. H.Y. Zhou, S.L. Zhang, Q.R. Yao,W.J. Li, *J. Alloys Compd*. 429 (2007) 116.
32. S. Orimo, H. Fujii, *Appl. Phys. A* 72 (2001) 167.